MDPI

Article

Experimental Study of the Shear Characteristics of Fault Filled with Different Types of Gouge in Underground Gas Storage

Guosheng Ding [1], Hejuan Liu [2,3], Debin Xia [2,3,*], Duocai Wang [4], Famu Huang [4], Haitao Guo [4], Lihuan Xie [2,3], Yintong Guo [2,3], Mingyang Wu [2,3] and Haijun Mao [2,3]

[1] PetroChina Research Institute of Exploration and Development//CNPC Key Laboratory of Oil & Gas Underground Storage, Beijing 100083, China
[2] State Key Laboratory of Geomechanics and Geotechnical Engineering, Institute of Rock and Soil Mechanics, Chinese Academy of Sciences, Wuhan 430071, China
[3] University of Chinese Academy of Sciences, Beijing 100049, China
[4] Pipe China West East Gas Pipeline Company, Shanghai 200120, China
* Correspondence: xiadebin21@163.com

Abstract: In the current international situation, energy storage is an important means for countries to stabilize their energy supply, of which underground storage of natural gas is an important part. Depleted gas reservoir type underground gas storage (UGS) has become the key type of gas storage to be built by virtue of safety and environmental protection and low cost. The multi-cycle high injection and production rate of natural gas in the depleted gas reservoir type UGS will cause the in-situ stress disturbance. The slip risk of fault in the geological system increases greatly compared with that before the construction of the storage engineering, which becomes a great threat to the sealing of the gas storage. Reasonable injection and production strategy depend on the reliable assessment of the shear behavior of the fault belt, which can guarantee the sealing characteristics of the UGS geological system and the efficient operation of the UGS. Therefore, the shear behavior of the fault is studied by carrying out experiments, which can provide important parameters for the evaluation of fault stability. However, there is a large gap between the rock samples used in the previous experimental study and the natural faults, and it is difficult to reflect the shear failure characteristics of natural faults. In this paper, similar fault models based on high-precision three-dimensional scanners and engraving machines, filled with three types of fault gouge, are prepared for a batch of representative direct shear tests. The results show that the peak shear strength of the fault rocks with a shear surface is higher than that of the fault rocks with a tensile surface. Compared with the clay mineral content, the roughness of the fault surface is much more significant for the shear strength of the fault rock. For the fault rocks with similar fault surface morphology, the higher the clay content in the fault gouge, the greater the shear strength of the fault rocks. For the fault rocks with different fault surface morphology and the same fault gouge, the cohesion and internal friction angle of the tensile type is generally smaller than that of the shear type.

Keywords: depleted gas storage; underground gas storage; filled fault; fault gouge; shear failure; 3D fractal dimension of roughness

1. Introduction

Underground storage of energy is an important strategic project for countries to cope with rising energy prices, ensure a secure energy supply and stable economic development, and make full use of underground space [1–3]. Depleted gas reservoirs are an important part of natural gas storage, generally converted from unconventional and shale gas reservoirs at the end of development [4]. This type of UGS is characterized by low permeability, strong non-homogeneity, deep burial, multi-phase fluid flow, and a complex mechanism of fluid–solid coupling [5,6] and is hydraulically fractured and modified at the initial stage of development [7–10]. This development method makes the geological

conditions complex after the transformation into a gas storage reservoir, containing more faults with tectonic fragmentation (shown in Figure 1), which poses a huge challenge to the long and stable operation of the gas storage reservoir and pressure expansion. The gas injection and production rate of the gas storage facility is several times higher than that during the development period. The multi-cycle, high-intensity injection, and production operation mode will affect the stability of the phase and the ability of natural gas adsorption analysis [11]. It will cause disturbance to the stability of the fault, easily trigger fault shear slip, and cause damage to the sealing performance of the gas storage facility [12]. There is a risk of inducing an earthquake [13]. Therefore, the study of fault shear characteristics can provide an important theoretical basis for gas storage construction, injection-production operating parameters, and capacity expansion design.
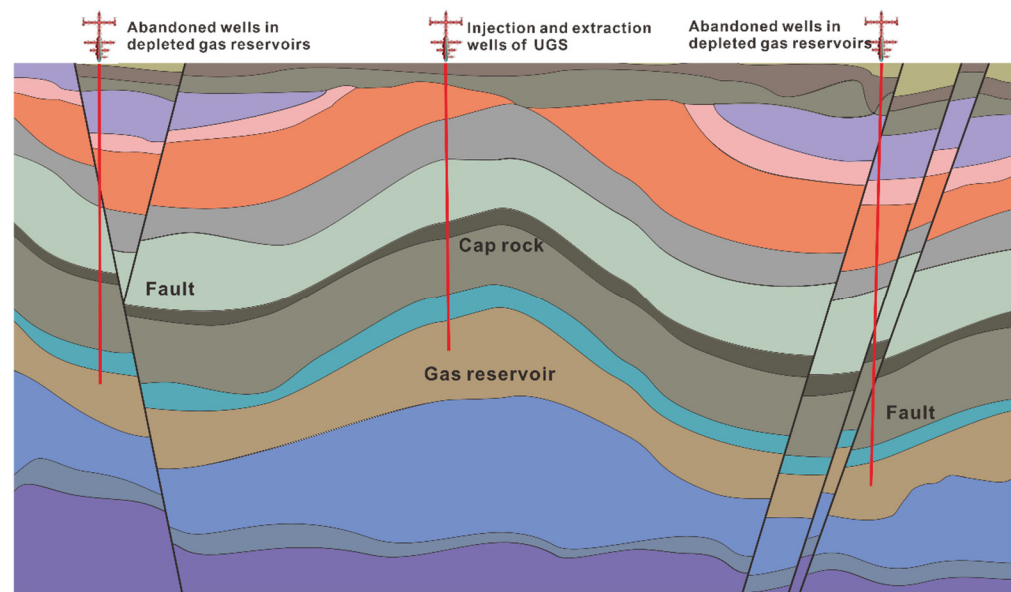

Figure 1. Schematic diagram of depleted gas reservoir type UGS.

To study the characteristics of fault shear slip, many scholars at home and abroad have conducted a lot of research work. These works mainly focus on unfilled fault rock samples and have achieved certain theoretical and experimental results. Wang [14] conducted laboratory experiments to examine how the crack propagation process, failure modes, and mechanical properties of the specimens were influenced by different flaw inclination angles, rock bridge lengths, and rock bridge inclination angles. The experimental results revealed that the specimens exhibited two types of failure modes: shear failure and tensile–shear failure, and the rock bridge coalescence modes could be classified into three categories: tensile crack coalescence, shear crack coalescence, and no coalescence. The peak strength of the specimens increased progressively with the increase of the rock bridge length and inclination angle, while it decreased gradually with the increase of the flaw inclination angle. The shear strength parameters (cohesion c and internal friction angle u) of the specimens varied nonlinearly with various factors (flaw angle, rock bridge length, and rock bridge angle).

Barton [15] made fault rock samples by splitting rock blocks for a direct shear test and found that the roughness of the fault plane will affect the shear strength and shear displacement. To study the shear behavior of jagged fault rock samples under different experimental conditions, Zhou et al. [16] made fault rock samples with different saw tooth heights and conducted experiments. The results show that the strength of the fault increases with the normal load and roughness height. As the shear rate increases, the strength of the joint first increases and then decreases. Jafari [17] used similar materials to replicate the rock samples of zigzag faults and natural faults and preliminarily analyzed the influence of the shear rate and normal stress on fault shear. Mirzaghorbanali [18] conducted a shear

test under constant normal stiffness through artificially prepared faults and discussed the influence of the shear rate and normal stress on the shear properties of joints. In terms of filled fault rocks, Xu Jiang [19] and other scholars carried out shear tests on unfilled structural surfaces and structural surfaces filled with gypsum, cuttings, and yellow mud. The results showed that the strength of the filling greatly affected the peak shear stress and normal displacement of the filled structural surfaces from filling gypsum and rock cuttings to yellow mud in descending order. Indraratna [20,21] and Papaliangas [22], through a series of shear tests on filled clay-type faults, pointed out that the thicker the filling, the smaller the shear strength of the structural plane rock, and when the filling degree of the structural plane rock reaches a certain after a critical value, its shear strength will depend entirely on the nature of the filling, and has nothing to do with the structural walls. In the numerical simulation, As'habi studied the peak strength and damage modes of fault rock samples under constrained and unconstrained conditions using discrete element numerical simulation methods. The results show that if the sample has one or two parallel joints, the strength obtained from the numerical method corresponds to the analytical model. However, if the sample has two intersecting symmetrical joints, the concentration of stress created at the vertices of the rock blocks increases the strength of the sample [23]. According to the shape of the fault surface and rock sample materials, the rock samples used by most scholars at home and abroad can be divided into three categories: ① regular jagged artificial faults; ② random surface morphology obtained by shearing or splitting intact rocks; ③ samples with the same surface morphology obtained from similar materials [24]. However, these three types of rock samples are quite different from real reservoir faults in terms of mechanical properties, fracture surface morphology, and roughness, and the experimental results are not representative enough. Therefore, it is of great significance to study the shear-slip mechanism of faults by preparing real natural fault planes in real rocks in batches.

In this paper, high-precision scanners and engraving machines were used to reproduce shear-type and tension-type faults in multiple rock samples. At the same time, three types of fault gouge with different clay mineral contents were arranged in the two faults to form fault rocks. The sample was used to study the effect of fault surface type and clay mineral content in fault gouge on shear characteristics.

2. Fault Rock Shear Experiment

In order to study the strength variation law and influencing factors of the shearing process of the two fault planes of the gas storage, this study uses the outcrop rock samples corresponding to the reservoir of the gas storage and uses three-dimensional shape scanning and high-precision engraving machine, which can reproduce a batch of rock samples with true shear and tension fault plane characteristics can avoid the influence of the difference in fault plane shape on the experimental results; at the same time, fault gouge is filled between the upper and lower fault planes to simulate the gas storage fault to the greatest extent.

2.1. Experimental Scheme Design

In this experiment, two types of fault planes (shear fracture and tensile fracture) were designed under three different clay mineral content fault gouge ratios (as shown in Table 1), under four different normal stresses (2 MPa, 4 MPa, 6 MPa, and 8 MPa) direct shear experiments to obtain cohesion, internal friction angle, and other parameters. According to these three parameters, 24 groups of experiments were designed, and the main parameters of the experiments are shown in Table 2:

Table 1. Composition of three kinds of fault gouge.

Fault Gouge Type	Mass Ratio	Clay Mineral Content (%)
NO. 1	Kaolin/Coarse particles/Montmorillonite/illite/Water/Hydroxypropyl Methyl Cellulose = 30:20:37.5:12.5:60:2	49.4
NO. 2	Kaolin/Coarse particles/Montmorillonite/illite/Water/Hydroxypropyl Methyl Cellulose = 30:30:30:10:60:2	43.2
NO. 3	Kaolin/Coarse particles/Montmorillonite/illite/Water/Hydroxypropyl Methyl Cellulose = 30:40:22.5:7.5:60:2	37

Table 2. Experimental design.

Fault Model	Experiment Number	Fault Gouge Type	Normal Stress (MPa)
Shear fault model	JQ-1	NO. 1	2
	JQ-2		4
	JQ-3		6
	JQ-4		8
	JQ-5	NO. 2	2
	JQ-6		4
	JQ-7		6
	JQ-8		8
	JQ-9	NO. 3	2
	JQ-10		4
	JQ-11		6
	JQ-12		8

2.2. Experimental Sample Preparation

2.2.1. Preparation of Fault Plane

First, the outcrop rock sample is processed into a cube with a side length of 50 mm and then put into the splitting device and the shearing box, respectively, and then the shearing box and the splitting device are placed in the RJST-616 shear box as shown in Figure 2. Experiments were carried out on the test bench, and under the action of certain parameters (as shown in Table 3), the initial shear fault plane and tension fault plane were obtained, as shown in Figure 3:
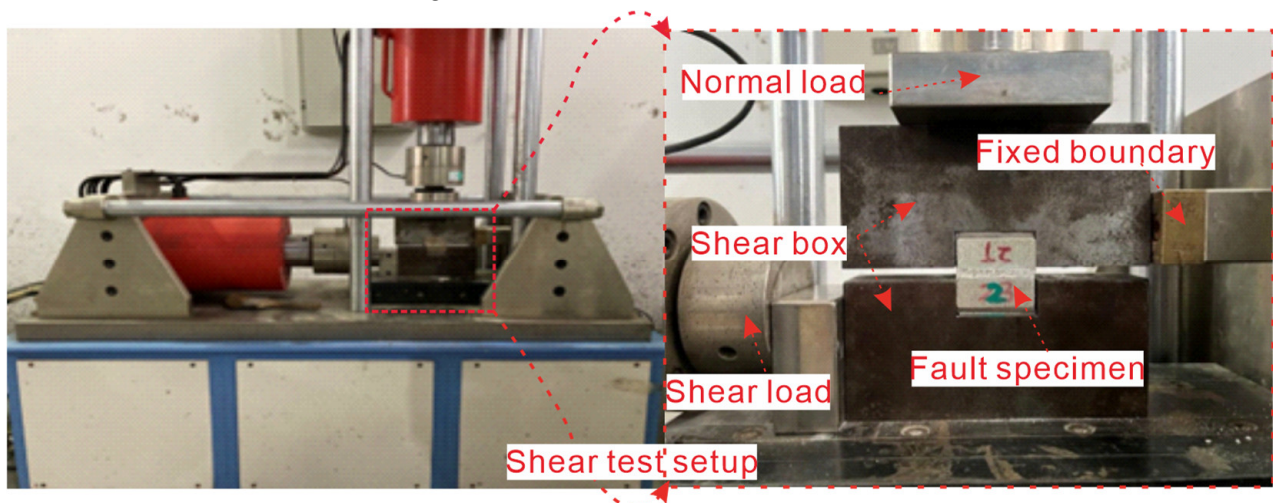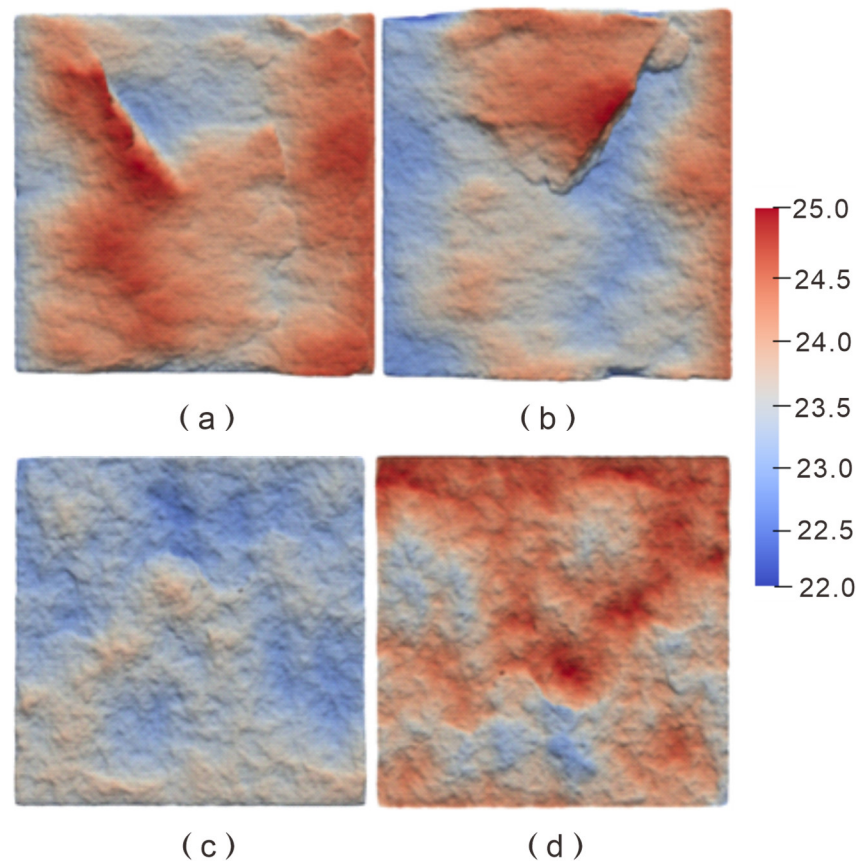

Figure 2. RJST-616 Shearing device.

Table 3. Experimental parameters of initial shear fault plane and tension fault plane.

Fault Model	Parameter	Normal	Tangential
Shear fault model	Displacement velocity	0.1 KN/s	1 mm/min
	Force/Displacement Target	15 KN	10 mm
Tension fault model	Displacement velocity	1 mm/min	\
	displacement target	10 mm	\

Figure 3. Initial fault plane ((**a**) is the upper surface of the shear fault model, (**b**) is the lower surface of the shear fault model, (**c**) is the upper surface of the tensile fault model, (**d**) is the lower surface of the tensile fault model).

It can be seen from Figure 3 that the fluctuation degree of the shear fault plane is relatively large, while the fluctuation degree of the tension fault plane is much smaller than that of the shear fault plane. To quantify the roughness of these two faults further, we use Equations (2)–(6) to calculate their fractal dimension, and the calculation results are 2.097 and 2.116, respectively, indicating that the roughness of the shear fault plane made in this paper is smaller than that of the tensile fault plane. Then, put the upper and lower fault planes on the turntable of the OKIO-5M high-precision 3D shape scanner, paste the reference points, scan, and obtain the 3D point cloud data of the fault plane after scanning. Import the point cloud data into the high-precision engraving machine and engrave a batch of fault rock samples containing real shear faults with the same shape and roughness, which is convenient for providing a rock sample basis for subsequent single-variable experimental research. The engraving process is as follows in Figure 4:
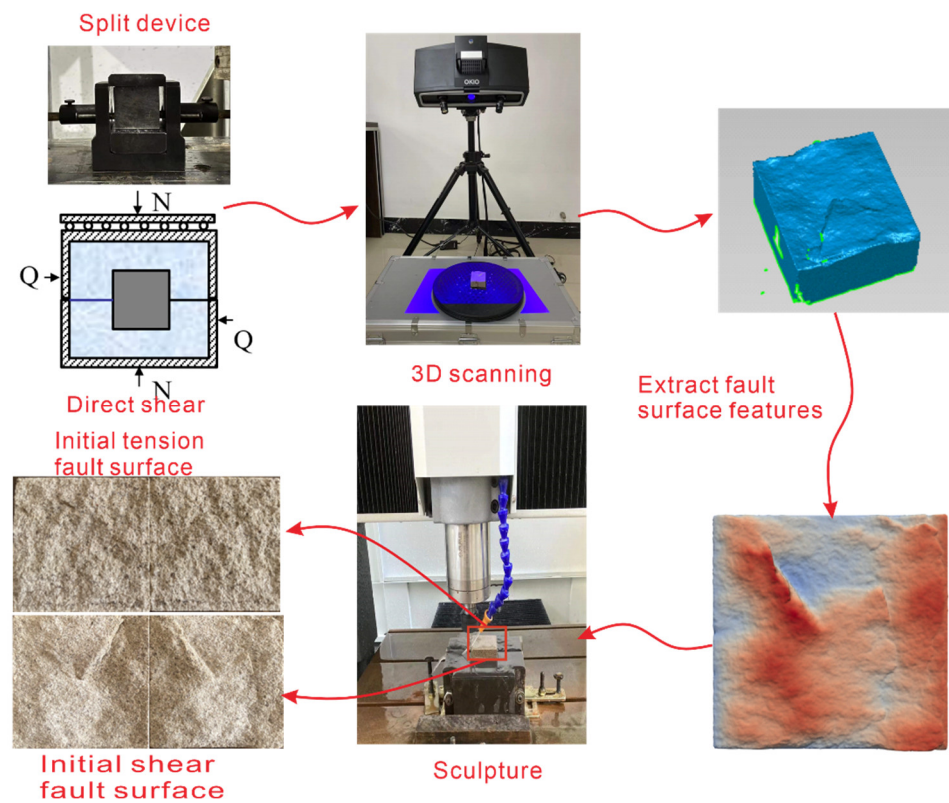
Figure 4. Fault plane re-engraving flow chart.

As shown in Figure 5, the rock sample is placed in the splitting device, and the position is adjusted using the adjustment bar. When the normal stress is applied, the upper and lower pillow pins in the device can play a stress concentration effect, which will split the rock sample along the middle.
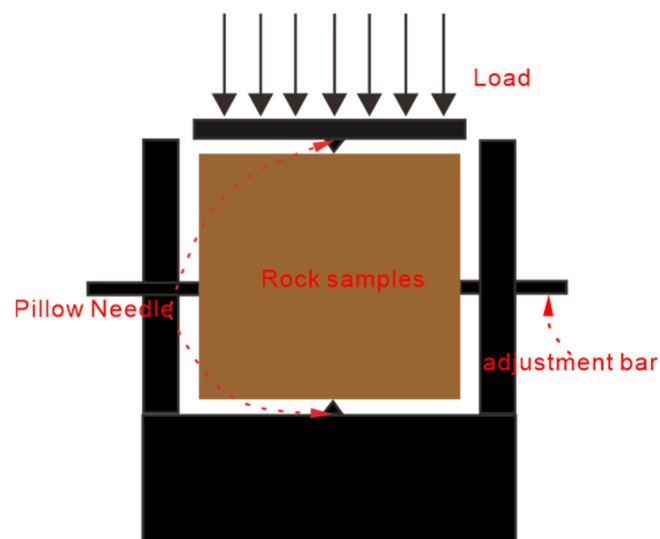

Figure 5. Schematic diagram of splitting device.

2.2.2. Fault Gouge Configuration

After making the fault plane, it is also necessary to evenly smear fault gouge on the upper and lower surfaces of the fault model to maximize the fault with the gas storage. The following are the configuration steps of fault mud:

① Dry the core and mineral powder that needs to be configured with fault gouge. After the core is dried, it needs to be weighed and recorded. This step is to obtain the content of the fault gouge in each sample after configuration.

② Weigh out various mineral powders in strict accordance with the proportion requirements (as shown in Figure 6), pour them into a container, and stir until the powder is uniform. Weigh the weight of pure water according to the water content, sprinkle it on the powder in batches, and stir while sprinkling until it is even. The observation of the microstructure of fault gouge by scanning electron microscope shows that there is a tight accumulation pattern between clay minerals and coarse particles; holes develop due to particle shedding (Figure 7).

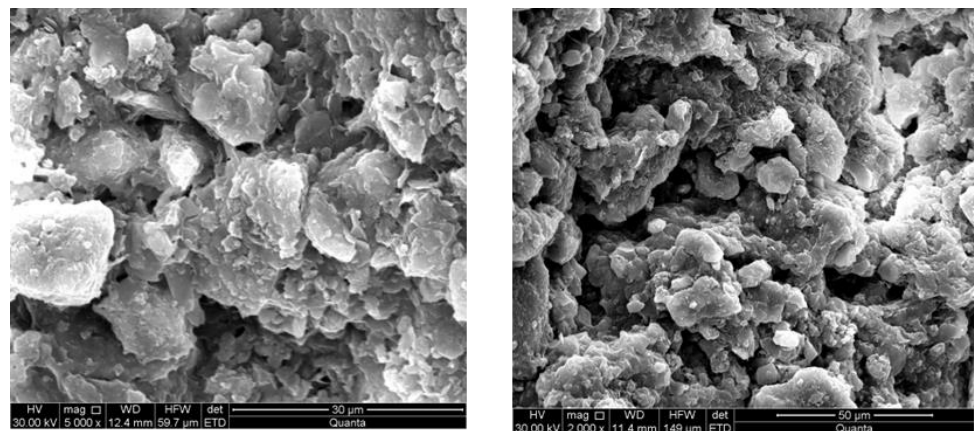**Figure 6.** Weigh all types of mineral powders required.

Figure 7. Microstructure of the No.1 fault gouge based on SEM.

③ Put the core into the mold. Put spacers under the cores to adjust the height so that the fault gouge thickness of each core is consistent, and then fix the cores. Use a steel ruler to spread the fault mud on the rock until it is flush with the surface of the mold. The spreading process is shown in Figure 8:

④ Put the samples containing fault gouge in an oven to dry, weigh and record after drying to ensure that the laying quality of the fault gouge remains within a certain range.

The fault model required for the experiment can be obtained according to the above-mentioned fault surface engraving and fault gouge configuration process, and the experimental sequence number is compiled according to the requirement. The prepared experimental model is shown in Figure 9:
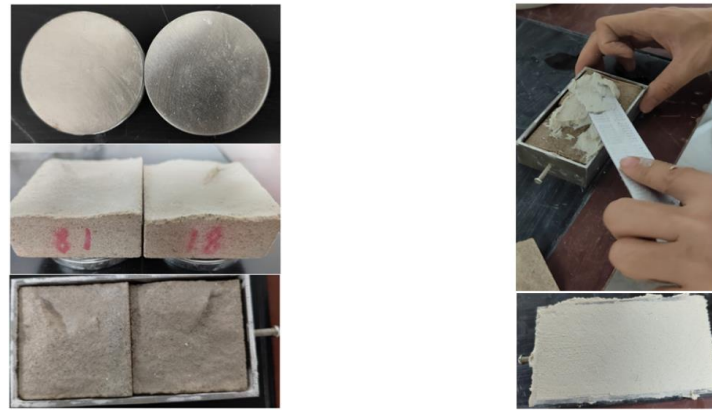
Figure 8. Fault gouge coating process.

(**a**)   (**b**)

Figure 9. The completed direct shear experiment sample. (**a**) is shear type experimental sample; (**b**) is a tensile type experimental sample.

2.3. Experimental Steps

Put the prepared experimental sample into the RJST-616 shear tester shown in Figure 9, set the experimental parameters according to the corresponding experimental design, and start the shearing experiment. The experimental steps are as follows:

① Take the dried sample out of the oven and cool it at room temperature for 12 h.

② Put the cooled sample on the RJST-616 shear tester platform, and place it in the upper and lower shear boxes, as shown in Figure 10:

Figure 10. Fault rocks placed in the RJST-616 direct shear apparatus.

③ According to the experimental design plan, set the corresponding normal parameters, the shear velocity is set to 1 mm/min, and the shear displacement is set to 6 mm;

④ First, preload vertically at a speed of 0.1 KN/S, stop after loading to a certain value (0.5 KN), then perform a horizontal pre-run, let the jack head touch the lower shear box,

and stop; then, run vertically, load the normal force to the value designed in the experiment. Finally, stop; run horizontally, at last, to carry out the shearing experiment; when the shearing displacement reaches the set 6 mm, the experiment will stop automatically.

⑤ Export the experimental data for analysis, retract the horizontal and vertical jacks, and unload the experimental samples to facilitate the next experiment.

⑥ Put the upper and lower parts of the rock sample into the scanner after the experiment, and scan the surface morphology of the fault after the experiment.

⑦ Repeat the process of ①~⑥ for all groups of experiments.

3. Analysis of Experimental Results

3.1. Effect of Different Normal Stresses on Shear Properties

In the fault model shear experiment, the same fault type, the same fault gouge ratio, and four different normal force shear deformation–shear force tangential curves are placed in one graph as one group, a total of six groups of shear the stress–shear displacement curves are shown in Figures 11 and 12. All six groups of curves rise sharply with the increase of shear displacement and then tend to level off; the curve shapes are basically consistent; both the peak shear strength and the residual strength increase with the increase of normal stress. This is because when the shear stress is less than the maximum shear stress under the experimental conditions, in the uniform increase in shear displacement of the experimental mode, the greater the need to overcome the frictional force, so the shear stress increases sharply; when the shear stress is equal to the maximum shear stress, to reach dynamic equilibrium, the shear stress is not increasing.
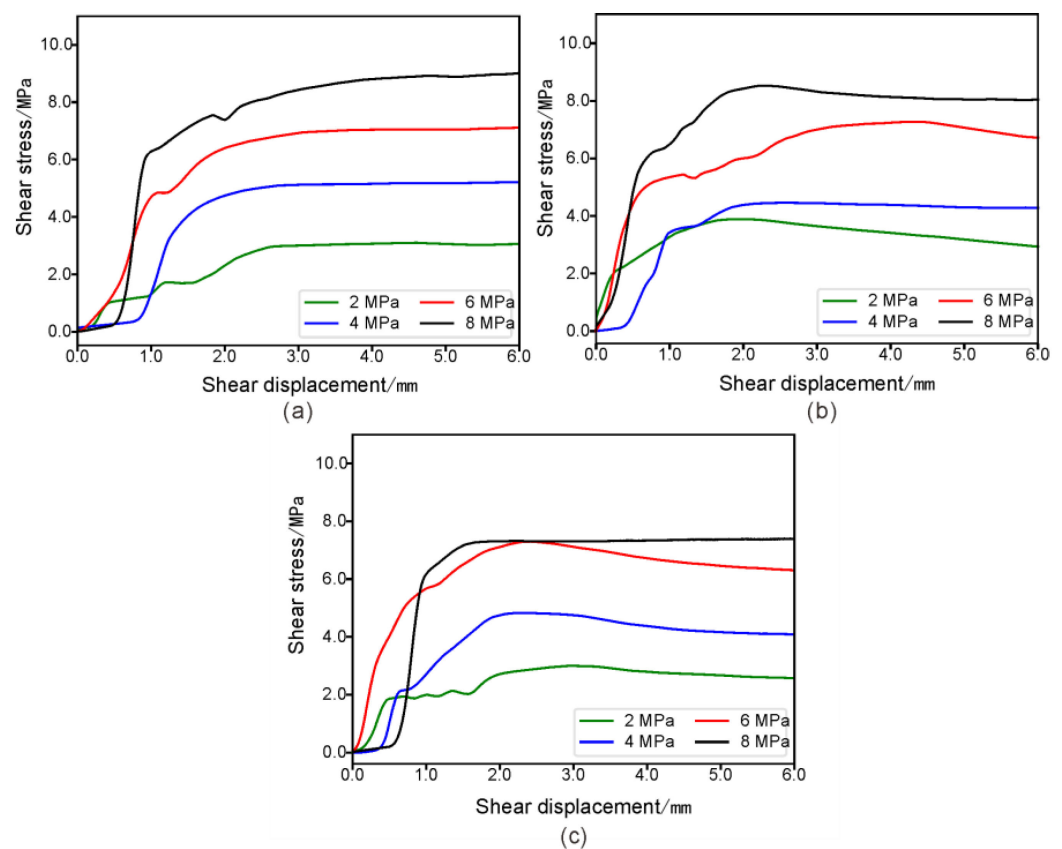

Figure 11. The shear stress–shear displacement curves for shear fault surface filled with 3 types of fault gouge ((**a**) is No. 1 fault gouge, (**b**) is No. 2 fault gouge, and (**c**) is No. 3 fault gouge).
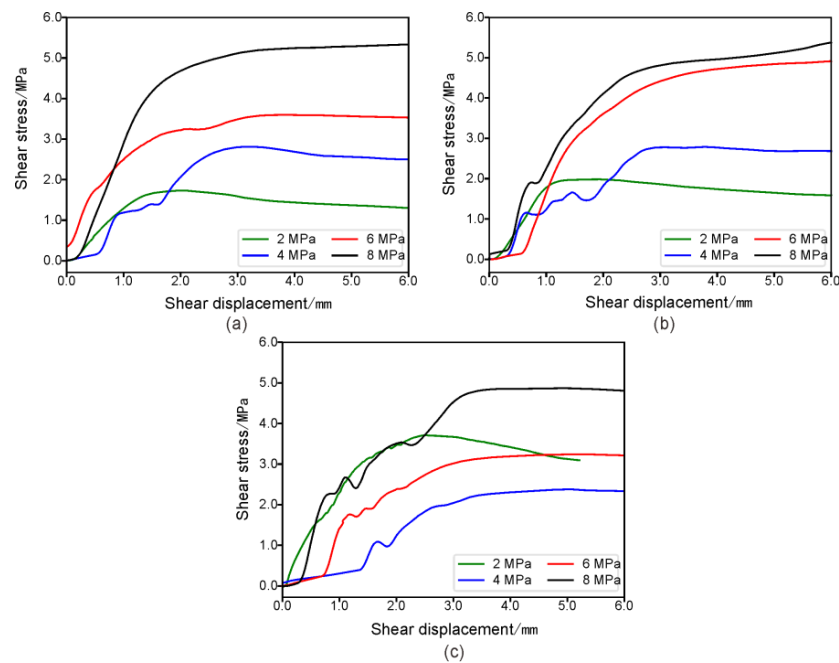
Figure 12. The shear stress–shear displacement curves of the tensile fault surface filled with three types of fault gouge ((**a**) is No. 1 fault gouge, (**b**) is No. 2 fault gouge, (**c**) is No. 3 fault gouge).

When the same type of fault gouge is laid, the peak shear strength of fault rocks with shear fault planes is significantly higher than that of tensional fault rocks (Figures 13 and 14) because the shear fault planes are concave and convex under the action of normal stress, the contact area between the upper and lower plates is larger than that of the tension fault plane, the peak shear strength of the fault rock samples of these two types of faults is roughly the same as that of the clay in the fault gouge decrease with a decrease in mineral content. Basically, the maximum shear stress increases with the normal stress.
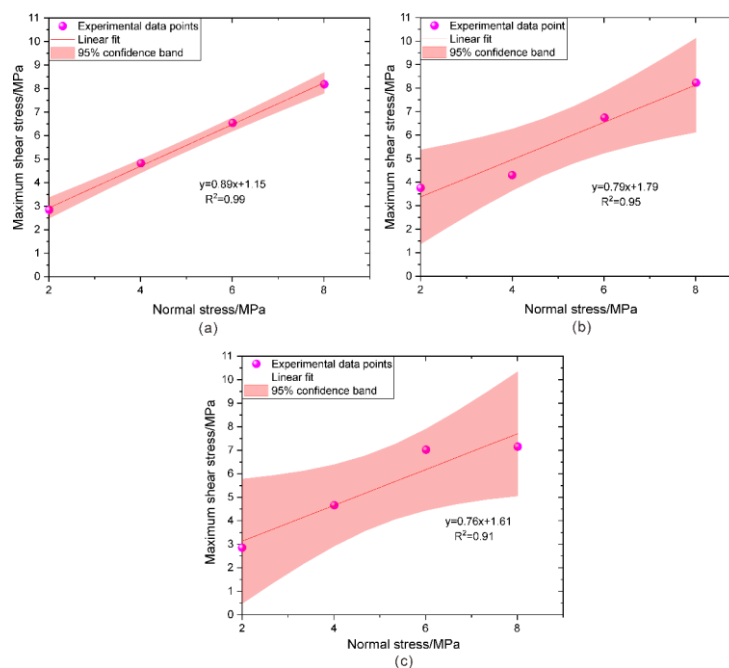

Figure 13. The linear fitting relationship between the shear strength and the normal stress of the fault rocks with three types of fault gouge ((**a**) is No. 1 fault gouge, (**b**) is No. 2 fault gouge, (**c**) is No. 3 fault gouge) and shear fault plane.
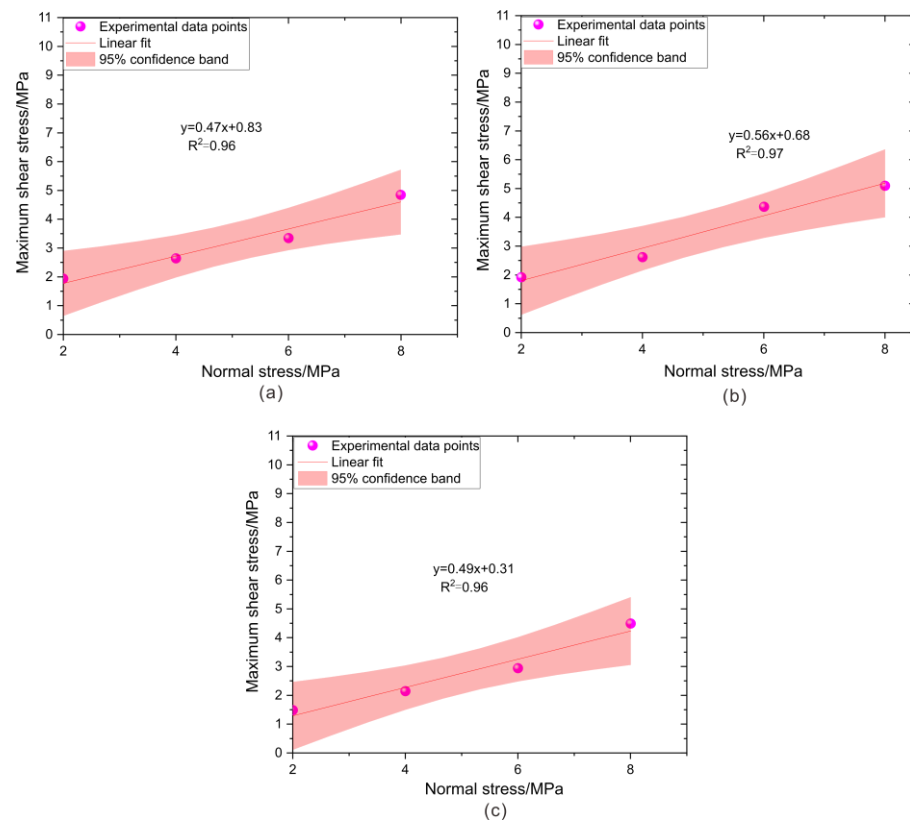
Figure 14. The linear fitting relationship between the shear strength and the normal stress of the fault rocks with three types of fault gouge ((**a**) is No. 1 fault gouge, (**b**) is No. 2 fault gouge, (**c**) is No. 3 fault gouge) and the tensile fault plane.

To further obtain the cohesive force and friction angle of these six groups of experiments, according to the Mohr–Coulomb criterion shear strength formula:

$$\tau = \sigma_n \tan \phi + c \tag{1}$$

where τ is the peak shear strength, MPa; σ_n is the normal stress, MPa; ϕ_b is the friction angle, °; c is the cohesive force, MPa.

The maximum shear stress and the corresponding normal stress obtained from these six sets of experiments were fitted, and the fitting trends are shown in Figures 13 and 14, from which it can be seen that the shear fault type and the tension fault type contain three kinds of fault gouge The linear correlation coefficients between shear strength and normal stress of fault rock samples are 0.99, 0.95, 0.91, 0.96, 0.97, and 0.96, respectively, all of which have strong correlations, indicating that the fitting degree of these six groups of curves is very high. Complies with the Mohr–Coulomb criterion. According to the shear strength principle of the Mohr–Coulomb criterion, the intercept, and slope of the fitting curve are the cohesion and friction angle of the fault rock sample. According to this method, two fault-type fault planes with three different configurations of fault gouge are obtained. The cohesion and friction angle of rock samples is shown in Table 4:
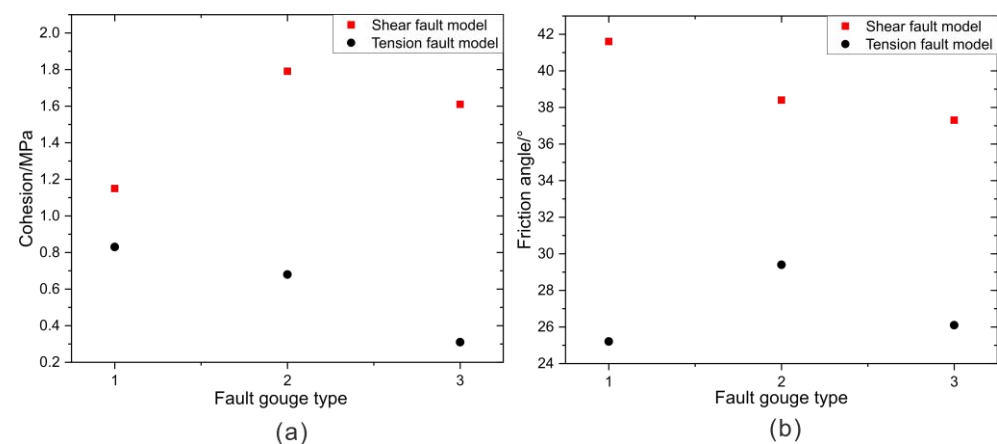
When the same type of fault gouge is laid, the cohesion and friction angle of the fault rocks with shear fault planes are significantly higher than those of tension fault rocks. This is because the shear fault surface has less roughness than the tension fault surface, while the maximum elevation difference is much larger than that of the tension fault surface. This makes the contact area of the rock fracture surface larger under the same normal stress conditions and thus requires more resistance to overcome, showing the cohesion and friction angle are greater.

Table 4. Cohesion and friction angle obtained from the direct shear tests of two types of fault rocks filled by different types of fault gouge.

Fault Model	Group Number	Cohesion (MPa)	Friction Angle (°)	Clay Mineral Content (%)
Shear fault model	Group 1	1.15	41.6	49.4
	Group 2	1.79	38.4	43.2
	Group 3	1.61	37.3	37.0
Tension fault model	Group 4	0.83	25.2	49.4
	Group 5	0.68	29.4	43.2
	Group 6	0.31	26.1	37.0

3.2. Effects of Different Clay Mineral Contents on the Shear Properties of Fault Rocks

It can be seen from Table 4 that different clay mineral contents have a great influence on the cohesion and friction angle, and the overall performance is as follows: with the decrease of clay mineral content, the cohesion and friction angle gradually decrease. To further analyze the influence of clay minerals on the shear stress–shear displacement curve, the curves of fault gouge with the same normal force and different clay mineral contents are drawn together, as shown in Figure 15. For fault rocks containing shear faults and tensional faults, at the same normal stress, the peak shear stress generally shows a decreasing trend as the content of clay minerals decreases. In fault gouge, the clay mineral component is very fine compared to other components of the fault gouge. When it is filled in the middle of the fault rock, it can effectively fill the gully between the fault planes and increase the contact surface between the upper and lower surfaces. Therefore, at a certain filling thickness, the greater the clay mineral content in the fault gouge, the larger the contact surface and the greater the shear strength.

Figure 15. Effect of fault gouge type on cohesion and friction angle. (**a**) is the relationship between cohesion and fault gouge type; (**b**) is the relationship between friction angle and fault gouge type.

3.3. Analysis of Fractal Dimension of Fault Surface Roughness

The elevation-based cube-covering method is widely used in the calculation of the fractal dimension of fault surface roughness. When using the cube covering method to measure a three-dimensional rough fracture surface, it is first necessary to mesh the space where the fault surface is located; then, the number of boxes corresponding to different sizes of boxes is obtained by the height value set method and the rounding method to calculate its roughness degree fractal dimension. According to the difference between the height value collection method and the rounding method, the current elevation-based cube covering methods can be divided into the conventional cubic covering method (CCM), improved cubic covering method (ICCM), difference differential cubic covering (DCCM) and relative difference cubic covering (RDCCM) [25–28].

However, these four calculation methods are not very stable for fault surfaces with different roughness. Therefore, a calculation method with better stability is proposed,

the stable difference cube covering method (SDCCM), and the grid diagram is shown in Figure 16, and its calculation formula is as follows:

$$S_{\text{hc}} = \{h_1(i,j), h_2(i,j+1), h_s(i+1,j), h_4(i+1,j+1)\} \tag{2}$$

$$h_{\max} = \max(S_{\text{hc}}), h_{\min} = \min(S_{\text{hc}}) \tag{3}$$

$$N_{i,j} = \text{INT}[(h_{\max} - h_{\min})/\delta] + 1 \tag{4}$$

$$N(\delta) = \sum_{i,j=1}^{n-1} N_{i,j} \tag{5}$$

$$D = -\lim_{\delta_i \to 0} \frac{\log(N(\delta_i))}{\log(\delta_i)} \tag{6}$$

where S_{hc} represents the height value set of the method, $N_{i,j}$ represents the number of boxes needed at the $\text{Grid}_{i,j}$ grid; $N(\delta)$ represents the number of boxes required to cover the entire fault plane; D is the fractal dimension of the fault surface roughness; δ_i is the size and length of the cube box unit;
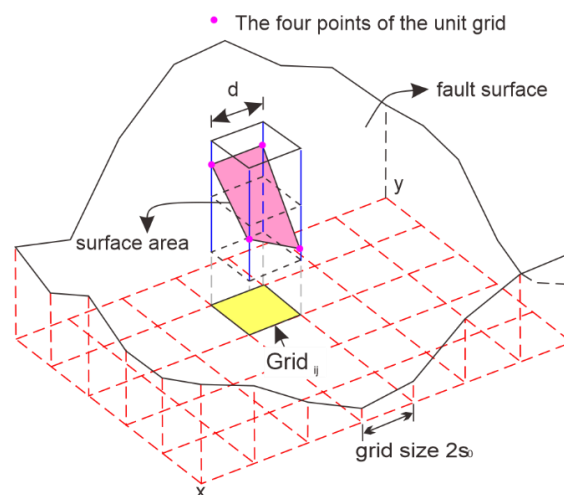

Figure 16. Schematic diagram of mesh division (Modified from Wu et al. [22]).

We used the Python programming language; the method is programmed, and after the sheared fault plane is scanned by a 3D shape scanner, the program is used to calculate the fractal dimension of the sheared fault plane roughness, and the calculation results are as shown in Figure 16:

It can be seen from Figure 17 that the fractal dimension of the roughness of the tension-type fault surface model is like that of the shear-type fault surface model after laying the same type of fault gouge shearing, and the difference is very small. This is because after laying the gouge, under the current experimental conditions, the shearing only occurs in the gouge laid in the middle, and the initial fault surface has not been sheared yet. It can be seen from Figure 17a,b that the type of fault gouge has no obvious effect on the roughness of the two models after shearing; it can be seen from Figure 17c,d that the two models The fractal dimension of roughness tends to decrease with the increase of normal stress. Under the same model and fault gouge test conditions, the greater the normal stress, the greater the compaction between the upper and lower plates of the fault model, and the stronger the interaction between the fault gouge during the direct shear process and the height of the change value is also smaller. Therefore, it can be concluded that the type of fault gouge

has no obvious effect on the post-shear roughness, but normal stress influences it. The rule is that the greater the normal stress, the smaller the fractal dimension of the roughness.
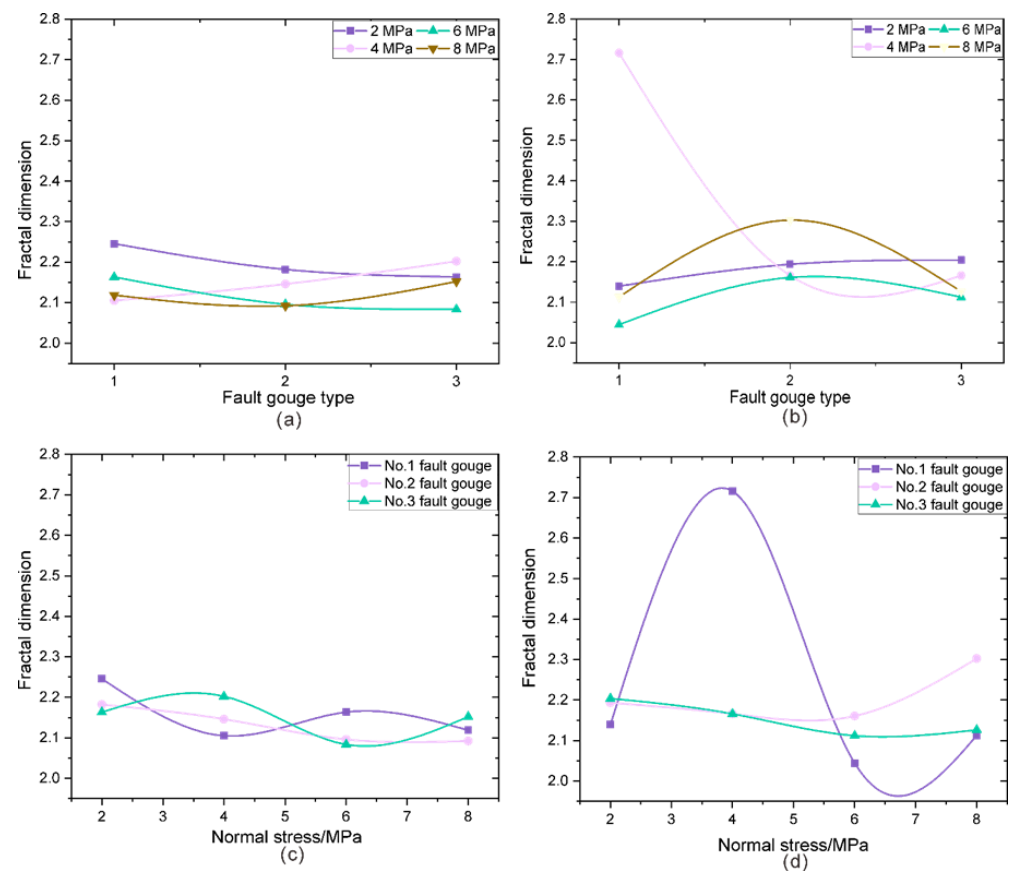

Figure 17. (**a**) The relationship between the fractal dimension of the shear fault and the type of fault gouge (**b**) The relationship between the fractal dimension of the tension fault and the type of fault gouge (**c**) The relationship between the fractal dimension of the shear fault and the normal stress (**d**) The relationship between the fractal dimension of the tension fault and the normal stress.

4. Conclusions

The contact mode of the fault surface and the nature of the weak filling (or fault gouge) within the fault have an important influence on the friction characteristics and fault movement of the fault. This paper considered two different types of fault surfaces (tensile type and shear type) and three different clay mineral contents of self-made fault gouge to study the law of shear properties of fault rocks, and some conclusions are obtained, as follows:

(1) High-precision engraving machines and high-precision 3D scanners are used to reproduce shear and tension faults, ensuring the comparability of faults. Fault rocks with different properties of fault gouge are closer to the properties of real fault zones.

(2) Under the same experimental conditions, the shear strength of the shear-type fault surface model is higher than that of the tensile-type fault surface model, which means that the tensile-type fault zone is more likely to slip and activate during the injection and production process of the gas reservoir. Compared with the influence of clay mineral content in fault gouges, the roughness of the fault plane has a greater influence on the shear strength of fault rocks.

(3) Within the same type of fault surface, the higher the clay mineral content in the fault gouge, the greater the shear strength of the fault rock.

(4) Under the same fault model and normal stress conditions, fault gouge has no obvious influence rule on the roughness of the shear fault surface; under the same fault model

and fault gouge conditions, the greater the normal stress, the smaller the roughness of the shear fault surface.

(5) Due to the limitations of the experimental equipment, the fault plane was set to a horizontal state, which differs somewhat from the actual fault plane. However, by converting the stress state and dip angle of the actual fault plane, a similar method can be used. When the fault dip angle is small and the stress on the ground is the same, the roughness of the contact surface after activation is relatively small. Therefore, in the construction and operation stages of gas storage tanks, it is necessary to focus on faults with small dip angles and tensile-type faults as much as possible.

References

1. Zhang, N.; Liu, W.; Zhang, Y.; Shan, P.; Shi, X. Microscopic pore structure of surrounding rock for underground strategic petroleum reserve (SPR) caverns in bedded rock salt. *Energies* **2020**, *13*, 1565. [CrossRef]
2. Liu, W.; Zhang, X.; Fan, J.; Li, Y.; Wang, L. Evaluation of potential for salt cavern gas storage and integration of brine extraction: Cavern utilization, Yangtze River Delta region. *Nat. Resour. Res.* **2020**, *29*, 3275–3290. [CrossRef]
3. Liu, W.; Zhang, Z.; Chen, J.; Jiang, D.; Wu, F.; Fan, J.; Li, Y. Feasibility evaluation of large-scale underground hydrogen storage in bedded salt rocks of China: A case study in Jiangsu province. *Energy* **2020**, *198*, 117348. [CrossRef]
4. Guo, Y.; Ying, Q.; Wang, D.; Zhang, H.; Huang, F.; Guo, H.; Xia, D. Experimental Study on Shear Characteristics of Structural Plane with Different Fluctuation Characteristics. *Energies* **2022**, *15*, 7563. [CrossRef]
5. Ding, G.; Wei, H. Review on 20 years' UGS construction in China and the prospect. *Oil Gas Storage Transp.* **2020**, *39*, 25–31.
6. Zhang, T.; Li, Y.; Sun, S.; Bai, H. Accelerating flash calculations in unconventional reservoirs considering capillary pressure using an optimized deep learning algorithm. *J. Pet. Sci. Eng.* **2020**, *195*, 107886. [CrossRef]
7. Wu, M.; Zhang, D.; Wang, W.; Li, M.; Liu, S.; Lu, J.; Gao, H. Numerical simulation of hydraulic fracturing based on two-dimensional surface fracture morphology reconstruction and combined finite-discrete element method. *J. Nat. Gas Sci. Eng.* **2020**, *82*, 103479. [CrossRef]
8. Wu, M.; Wang, W.; Song, Z.; Liu, B.; Feng, C. Exploring the influence of heterogeneity on hydraulic fracturing based on the combined finite–discrete method. *Eng. Fract. Mech.* **2021**, *252*, 107835. [CrossRef]
9. Xia, D.; Yang, Z.; Li, D.; Zhang, Y.; He, Y.; Luo, Y.; Zhao, X. Evaluation Method of the Vertical Well Hydraulic Fracturing Effect Based on Production Data. *Geofluids* **2021**, *21*, 1–12. [CrossRef]
10. Xia, D.; Yang, Z.; Gao, T.; Li, H.; Lin, W. Characteristics of micro-and nano-pores in shale oil reservoirs. *J. Pet. Explor. Prod.* **2021**, *11*, 157–169. [CrossRef]
11. Zhang, T.; Sun, S. A coupled Lattice Boltzmann approach to simulate gas flow and transport in shale reservoirs with dynamic sorption. *Fuel* **2019**, *246*, 196–203. [CrossRef]
12. Zheng, Y.; Sun, J.; Qiu, X.; Lai, X.; Liu, J.; Guo, Z.; Min, Z. Connotation and evaluation technique of geological integrity of UGSs in oil/gas fields. *Nat. Gas Ind. B* **2020**, *7*, 594–603. [CrossRef]
13. Liu, H.; Tong, R.; Hou, Z.; Dou, B.; Mao, H.; Huang, G. Review of Induced Seismicity Caused by Subsurface Fluid Injection and Production and Impacts on the Geothermal Energy Production from Deep High Temperature Rock. *Adv. Eng. Sci.* **2022**, *54*, 83–96.
14. Wang, W.; Sun, S.; Le, H.; Shu, Y.; Zhu, F.; Fan, H.; Liu, Y. Experimental and numerical study on failure modes and shear strength parameters of rock-like specimens containing two infilled flaws. *Int. J. Civ. Eng.* **2019**, *17*, 1895–1908. [CrossRef]
15. Barton, N.R. A model study of rock-joint deformation. *Int. J. Rock Mech. Min. Sci. Geomech. Abstr.* **1972**, *9*, 579–582. [CrossRef]
16. Zhou, H.; Meng, F.; Zhang, C.; Hu, D.; Lu, J.; Xu, R. Investigation of the acoustic emission characteristics of artificial saw-tooth joints under shearing condition. *Acta Geotech.* **2016**, *11*, 925–939. [CrossRef]
17. Jafari, M.; Hosseini, K.; Pellet, F.; Boulon, M.; Buzzi, O. Evaluation of shear strength of rock joints subjected to cyclic loading. *Soil Dyn. Earthq. Eng.* **2003**, *23*, 619–630. [CrossRef]
18. Mirzaghorbanali, A.; Nemcik, J.; Aziz, N. Effects of Shear Rate on Cyclic Loading Shear Behaviour of Rock Joints Under Constant Normal Stiffness Conditions. *Rock Mech. Rock Eng.* **2014**, *47*, 1931–1938. [CrossRef]

19. Xu, J.; Lei, J.; Liu, Y.; Wu, J. Experimental study on shear behavior of joints filled with different materials. *Rock Soil Mech.* **2019**, *40*, 4129–4137.
20. Indraratna, B.; Oliveira, D.; Brown, E. A Shear-Displacement Criterion for Soil-Infilled Rock Discontinuities. *Geotechnique* **2010**, *60*, 623–633. [CrossRef]
21. Indraratna, B.; Oliveira, D.; Brown, E.; De Assis, A. Effect of soil–infilled joints on the stability of rock wedges formed in a tunnel roof. *Int. J. Rock Mech. Min. Sci.* **2010**, *47*, 739–751. [CrossRef]
22. Papaliangas, T.; Hencher, S.; Lumsden, A.; Manolopoulou, S. The effect of frictional fill thickness on the shear strength of rock discontinuities. *Int. J. Rock Mech. Min. Sci. Geomech. Abstr.* **1993**, *30*, 81–91. [CrossRef]
23. As'Habi, F.; Lakirouhani, A. Numerical modeling of jointed rock samples under unconfined and confined conditions to study peak strength and failure mode. *Arab. J. Geosci.* **2021**, *14*, 3. [CrossRef]
24. Liu, C.; Jiang, Q.; Xin, J.; Wu, S.; Liu, J.; Gong, F. Shearing damage evolution of natural rock joints with different wall strengths. *Rock Mech. Rock Eng.* **2022**, *55*, 1599–1617. [CrossRef]
25. Wu, M.; Wang, W.; Shi, D.; Song, Z.; Li, M.; Luo, Y. Improved box-counting methods to directly estimate the fractal dimension of a rough surface. *Measurement* **2021**, *177*, 109303. [CrossRef]
26. Zhou, H.; Xie, H. Direct estimation of the fractal dimensions of a fracture surface of rock. *Surf. Rev. Lett.* **2003**, *10*, 751–762. [CrossRef]
27. Zhang, Y.; Zhou, H.; Xie, H. Improved cubic covering method for fractal dimensions of a fracture surface of rock. *Chin. J. Rock Mech. Eng.* **2005**, *24*, 3192–3196.
28. Ai, T.; Zhang, R.; Zhou, H.; Pei, J. Box-counting methods to directly estimate the fractal dimension of a rock surface. *Appl. Surf. Sci.* **2014**, *314*, 610–621. [CrossRef]